Cell Reports Medicine, Volume *5*

Supplemental information

Pharmacological induction of chromatin remodeling drives chemosensitization in triple-negative breast cancer

Meisam Bagheri, Gadisti Aisha Mohamed, Mohammed Ashick Mohamed Saleem, Nevena B. Ognjenovic, Hanxu Lu, Fred W. Kolling, Owen M. Wilkins, Subhadeep Das, Ian S. LaCroix, Shivashankar H. Nagaraj, Kristen E. Muller, Scott A. Gerber, Todd W. Miller, and Diwakar R. Pattabiraman

Uniprot protein name	Accession #	Hyperlink	delta-Sm
NFAC4_MOUSE	Q8K120	Q8K120	2.576
CARD9_MOUSE	A2AIV8	A2AIV8	2.463
CRNL1_MOUSE	P63154	P63154	2.352
BUB1_MOUSE	O08901	O08901	2.338
CDCA5_MOUSE	Q9CPY3	Q9CPY3	2.060
MK67I_MOUSE	Q91VE6	Q91VE6	1.827
DOCK6_MOUSE	Q8VDR9	Q8VDR9	1.824
SOSD1_MOUSE	Q9CQN4	Q9CQN4	1.810
FL2D_MOUSE	Q9ER69	Q9ER69	1.736
KI20A_MOUSE	P97329	P97329	1.715
CRIP3_MOUSE	Q6Q6R3	Q6Q6R3	1.671
CDNF_MOUSE	Q8CC36	Q8CC36	1.629
RGAP1_MOUSE	Q9WVM1	Q9WVM1	1.622
HNRL2_MOUSE	Q00PI9	Q00PI9	1.602
TOM22_MOUSE	Q9CPQ3	Q9CPQ3	1.552
MYO1H_MOUSE	Q9D6A1	Q9D6A1	1.494
MYO15_MOUSE	Q9QZZ4	Q9QZZ4	1.472
MYO7A_MOUSE	P97479	P97479	1.472
MYO7B_MOUSE	Q99MZ6	Q99MZ6	1.472
HNRPC_MOUSE	Q9Z204	Q9Z204	1.465
UB2E2_MOUSE	Q91W82	Q91W82	1.459
UB2E3_MOUSE	P52483	P52483	1.459
TERT_MOUSE	O70372	O70372	1.445
BAZ1B_MOUSE	Q9Z277	Q9Z277	1.433
PIMRE_MOUSE	Q8BFY7	Q8BFY7	1.420
MYO1D_MOUSE	Q5SYD0	Q5SYD0	1.352
H2A2B_MOUSE	Q64522	Q64522	1.327
RALY_MOUSE	Q64012	Q64012	1.311
SMRD1_MOUSE	Q61466	Q61466	1.309
SMRD3_MOUSE	Q6P9Z1	Q6P9Z1	1.309
RIOX1_MOUSE	Q9JJF3	Q9JJF3	1.290
EBP2_MOUSE	Q9D903	Q9D903	1.267
K1C19_MOUSE	P19001	P19001	1.081
CCNB1_MOUSE	P24860	P24860	1.030
CENPE_MOUSE	Q6RT24	Q6RT24	0.896
SOGA3_MOUSE	Q6NZL0	Q6NZL0	0.889
LEMD2_MOUSE	Q6DVA0	Q6DVA0	0.883
PERI_MOUSE	P15331	P15331	0.841
SRPRB_MOUSE	P47758	P47758	0.705
MUC2_MOUSE	Q80Z19	Q80Z19	0.580

Supplementary Table S1: Proteins with stability significantly altered by eribulin treatment in PB3 cells. Cells were treated +/- 300 nM eribulin for 4 h, and protein extracts were analyzed by PISA. Protein stability ratios vs. control are reported as delta-Sm values. The 40 proteins with delta-Sm >0.5 and $p<0.05$ are listed. Related to Figure 5.

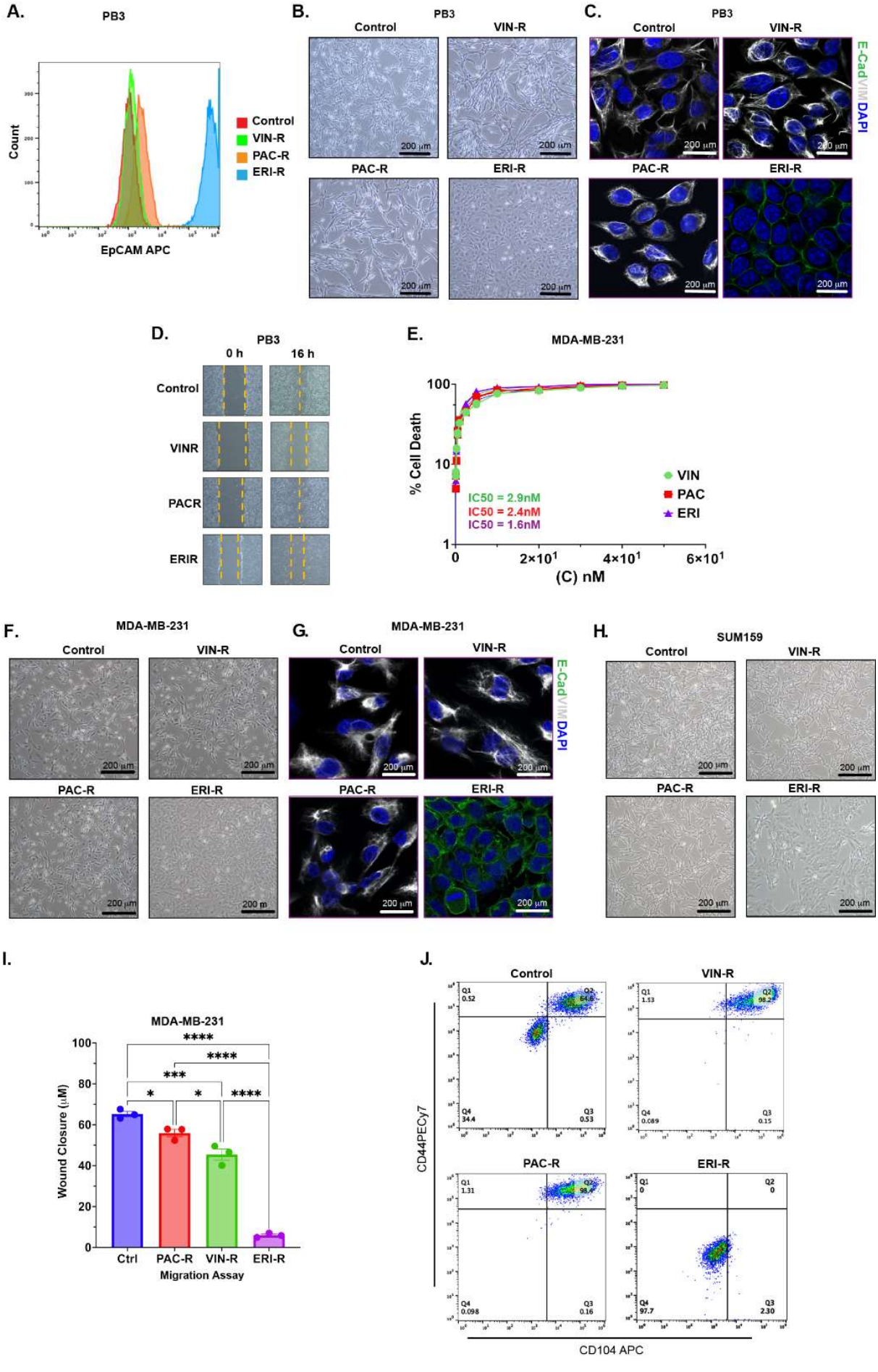
A.
PB3
Count
EpCAM APC
Control
VIN-R
PAC-R
ERI-R
B.
PB3
Control
VIN-R
PAC-R
ERI-R
200 µm
C.
PB3
Control
VIN-R
PAC-R
ERI-R
E-Cad/VIN DAPI
200 µm
D.
PB3
0 h
16 h
Control
VINR
PACR
ERIR
E.
MDA-MB-231
% Cell Death
100
10
1
0
2×10¹
4×10¹
6×10¹
(C) nM
IC50 = 2.9nM
IC50 = 2.4nM
IC50 = 1.6nM
VIN
PAC
ERI
F.
MDA-MB-231
Control
VIN-R
PAC-R
ERI-R
200 µm
G.
MDA-MB-231
Control
VIN-R
PAC-R
ERI-R
E-Cad/VIN DAPI
200 µm
H.
SUM159
Control
VIN-R
PAC-R
ERI-R
200 µm
I.
MDA-MB-231
Wound Closure (µM)
100
80
60
40
20
0
****
****
***
*
*
****
Ctrl
PAC-R
VIN-R
ERI-R
Migration Assay
J.
Control
VIN-R
PAC-R
ERI-R
CD44PECy7
CD104 APC
Q1 0.52
Q2 64.6
Q4 34.4
Q3 0.53
Q1 1.53
Q2 98.2
Q4 0.089
Q3 0.15
Q1 1.31
Q2 98.7
Q4 0.098
Q3 0.16
Q1 0
Q2 0
Q4 97.7
Q3 2.30

Supplementary Figure S1: Eribulin induces MET in TNBC cells. (A) Flow cytometry-based quantification of EpCAM expression in PB3 parental cells and drug-resistant derivatives. **(B/C)** Estimation of EMT state of PB3 cells and drug-resistant derivatives by morphological assessment in brightfield images (B), and immunofluorescence for E-cadherin (green) and vimentin (white) (C). **(D)** A monolayer scratch assay was carried out in PB3 cells and drug-resistant derivatives to assess invasive properties over 16 h. **(E)** Dose-response curves of MDA-MB-231 cells were generated to calculate IC_{50} values for eribulin, paclitaxel, and vinorelbine. **(F/G)** Estimation of EMT state of MDA-MB-231 cells and drug-resistant derivatives as in (B/C). **(H)** Estimation of EMT state of SUM159 cells and drug-resistant derivatives as in (B). **(I)** A monolayer scratch assay was carried out in MDA-MB-231 cells and drug-resistant derivatives to assess the invasive properties over 16 h. *$p<0.05$, ***$p<0.0005$, ****$p<0.0001$ by Tukey-adjusted pairwise comparison. **(J)** Flow cytometry-based quantification of CD104 and CD44 expression in MDA-MB-231 parental cells and drug-resistant derivatives. Related to Figure 1.

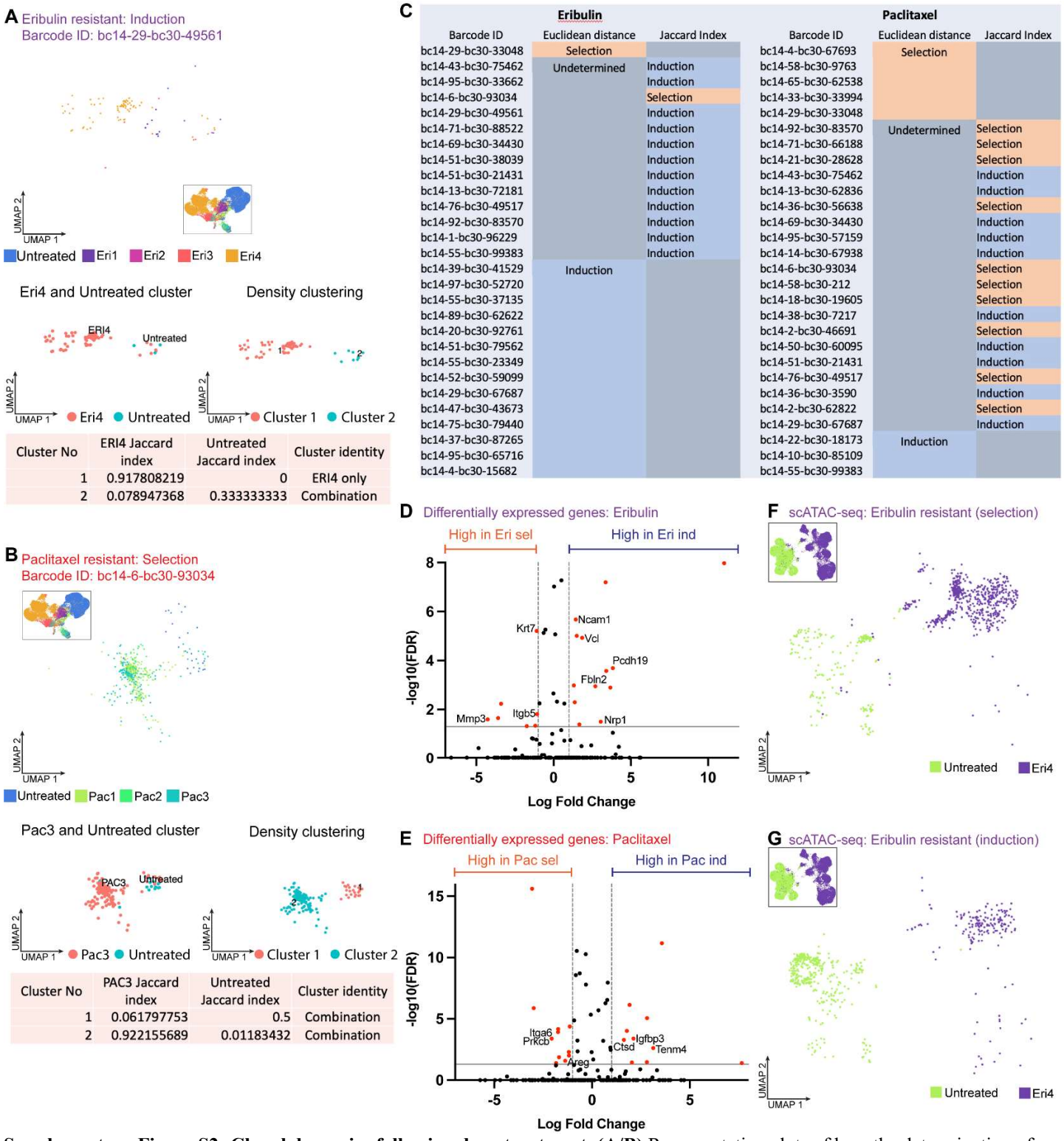

Cluster No	ERI4 Jaccard index	Untreated Jaccard index	Cluster identity
1	0.917808219	0	ERI4 only
2	0.078947368	0.333333333	Combination

Cluster No	PAC3 Jaccard index	Untreated Jaccard index	Cluster identity
1	0.061797753	0.5	Combination
2	0.922155689	0.01183432	Combination

Supplementary Figure S2: Clonal dynamics following drug treatment. (A/B) Representative plots of how the determination of selection vs. induction was made based on Jaccard Index. In (A), cells with a single genetic barcode are shown as an example. The representative plot (top) reveals a combination of induction and selection for this barcode: some clusters are resistant by induction (i.e., no untreated cells in the final treatment cluster), and other clusters are resistant by selection (i.e., at least one untreated cell in the ERI4 final treatment cluster). For reference, the inset shows the plot from all barcodes (reproduced from Figure 3B). The cluster with the largest number of drug-resistant cells was used to determine the mode of resistance for a given cell line/derivative. In this example, Cluster No. 1 (pink dots in lower right plot) has the largest number of ERI4 cells (pink dots in lower left plot), and these cells are resistant by induction; therefore, this barcode was assigned as resistant by induction. **(B)** Representative plots of barcodes resistant by selection. Untreated cells and PAC3 cells with the same barcode share the same clusters as observed by the Jaccard index score. **(C)** Levels of induction or selection were determined by breakdown of both Euclidean distance and Jaccard index calculations. Representative data are shown. **(D/E)** Volcano plots showing differentially expressed genes that may predict induction or selection

resistance upon eribulin (D) and paclitaxel (E) treatment. Gene expression profiles of (i) untreated cells with the same barcode as eribulin induction-resistant cells and paclitaxel induction-resistant cells (highest 10 Euclidean distance values) were compared against (ii) untreated cells with the same barcode as eribulin selection-resistant and paclitaxel selection-resistant cells (lowest 10 Euclidean distance values). Significant genes were determined by FDR <0.05 and fold-change >2. **(F/G)** scATAC-seq UMAP projection of (F) untreated and eribulin-resistant cells by selection, and (G) untreated and eribulin-resistant cells resistant by induction (highest 10 Euclidean distance values). Related to Figure 3.

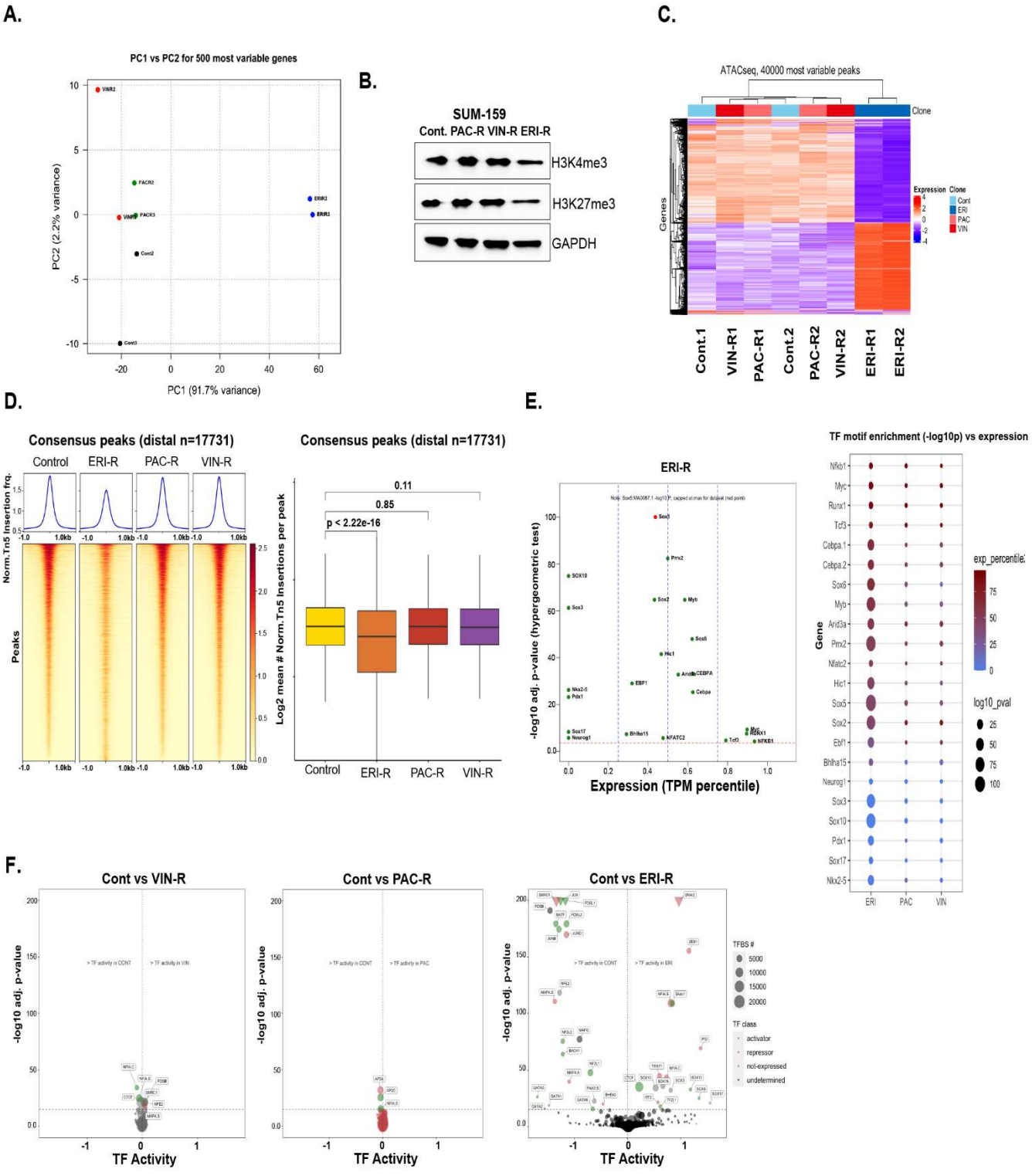

Supplementary Figure S3: Eribulin induces a shift in chromatin profile of TNBC cells. (A) Principal Components Analysis (PCA) of the 500 most variably expressed genes between PB3 parental and drug-resistant cells analyzed by bulk RNA-seq. **(B)** Immunoblotting of lysates from SUM159 parental and drug-resistant cells. **(C-E)** Bulk ATAC-seq was performed using PB3 parental and drug-resistant cells. Differences in chromatin accessibility are depicted as a heat map of the most variable peaks (C), and peak accessibility surrounding consensus distal-associated regions (D). Panel (E) shows transcription factor (TF) motifs (de-)enriched in PB3$^{ERI\text{-}R}$ cells. (*Left*) The x-axis shows target gene expression, and the y-axis shows -$\log_{10}$(p-value) of each TF. (*Right*) TF motif enrichment over target expression. Circle size indicates p-value, and circle color indicates percentile expression of target genes. **(F)** Advanced volcano plot of active and inactive TFs determined by diffTF from ATAC-seq. TF classification is displayed as circle color, and number of TF binding sites used to determine TF activity is displayed as circle size. Related to Figure 4.

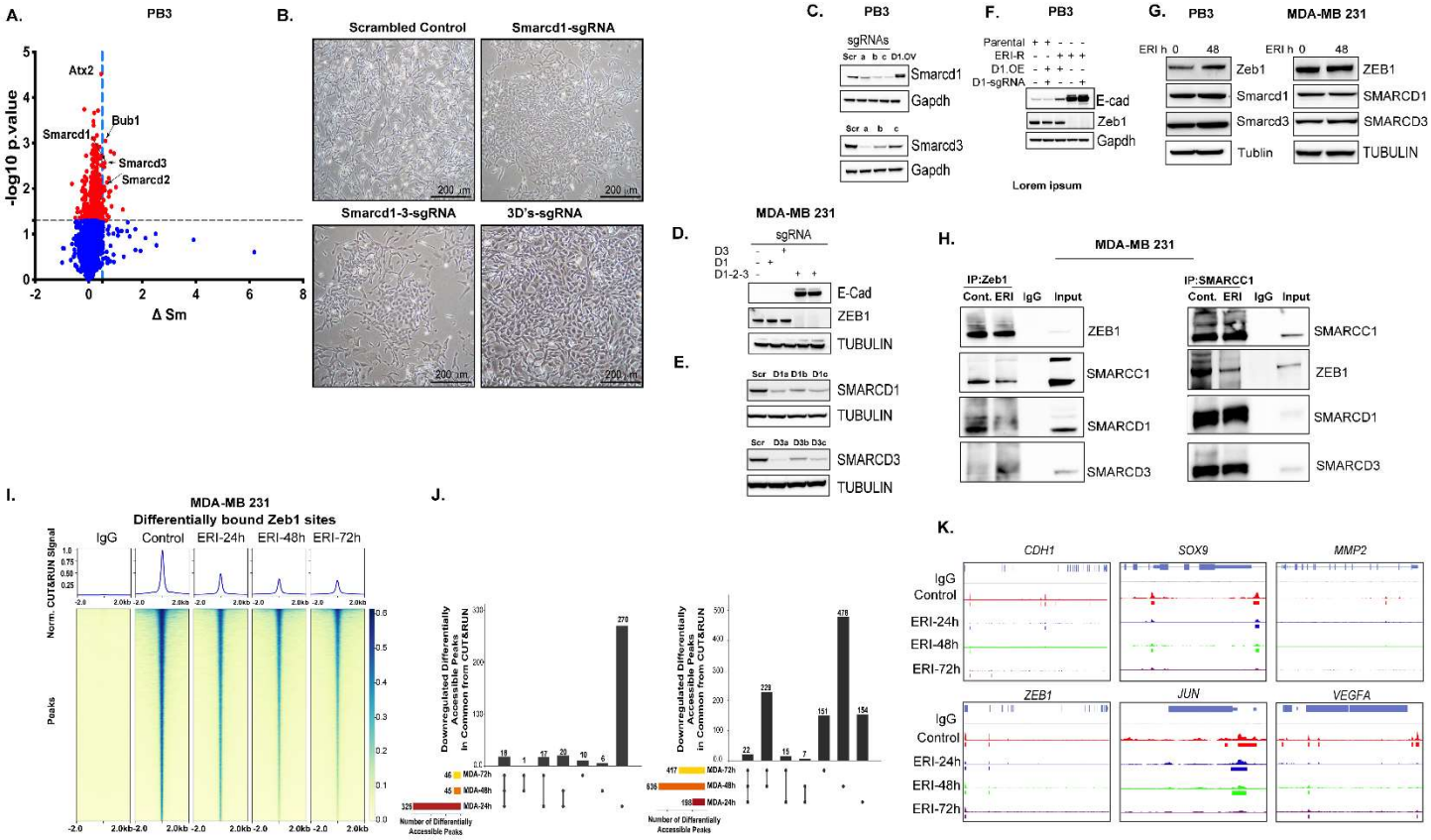

Supplementary Figure S4: ZEB1-SWI/SNF interactions are necessary for maintenance of a mesenchymal state. (A) Proteome Integral Solubility Alteration (PISA) assay of PB3 cells treated +/- 300 nM eribulin for 4 h to explore protein targets of eribulin. Proteins with DSm >0.5 and p<0.05 (t-test) compared to control were prioritized. **(B)** Estimation of EMT state by morphological assessment of brightfield images of PB3 cells with knockout of *Smarcd1*, *Smarcd3*, *Smarcd1/2/3*, or scrambled control. **(C)** Immunoblot validation of CRISPR/Cas9-mediated knockout of *Smarcd1* in PB3 cells using 3 different sgRNAs (a, b, c). The right lane provides confirmation of overexpression of exogenous Smarcd1. **(D)** Immunoblot analysis of EMT markers in MDA-MB-231 cells with knockout of *SMARCD1*, *SMARCD3*, or *SMARCD1/2/3*. **(E)** Immunoblot validation of CRISPR/Cas9-mediated knockout of *SMARCD1* or *SMARCD3* in MDA-MB-231 cells using 3 different sgRNAs (a, b, c). **(F)** Immunoblot analysis of PB3 parental and ERI-R cells with knockout (KO) or overexpression (OE) of Smarcd1. Drug was withdrawn at least 72 h prior to seeding for assay. **(G)** Cells were treated +/- eribulin for 48 h, and lysates were analyzed by immunoblot. **(H)** MDA-MB-231 cells were treated +/- eribulin for 48 h. Lysates and immunoprecipitates (anti-ZEB1, anti-SMARCC1, or IgG control) were analyzed by immunoblot. **(I-K)** Genome-wide occupancy of ZEB1 binding sites in MDA-MB-231 cells treated with eribulin for 0, 24, 48, or 72 h was determined by CUT&RUN. Shown in (I) are the average CUT&RUN enrichment profile (*top*) and heatmap illustrating the CUT&RUN signal +/- 2 kb of peaks (*bottom*). UpSet plots of differentially accessible peaks at the indicated time points are shown in (J). Panel (K) shows signal tracks of Zeb1 target gene chromatin accessibly. Related to Figure 5.

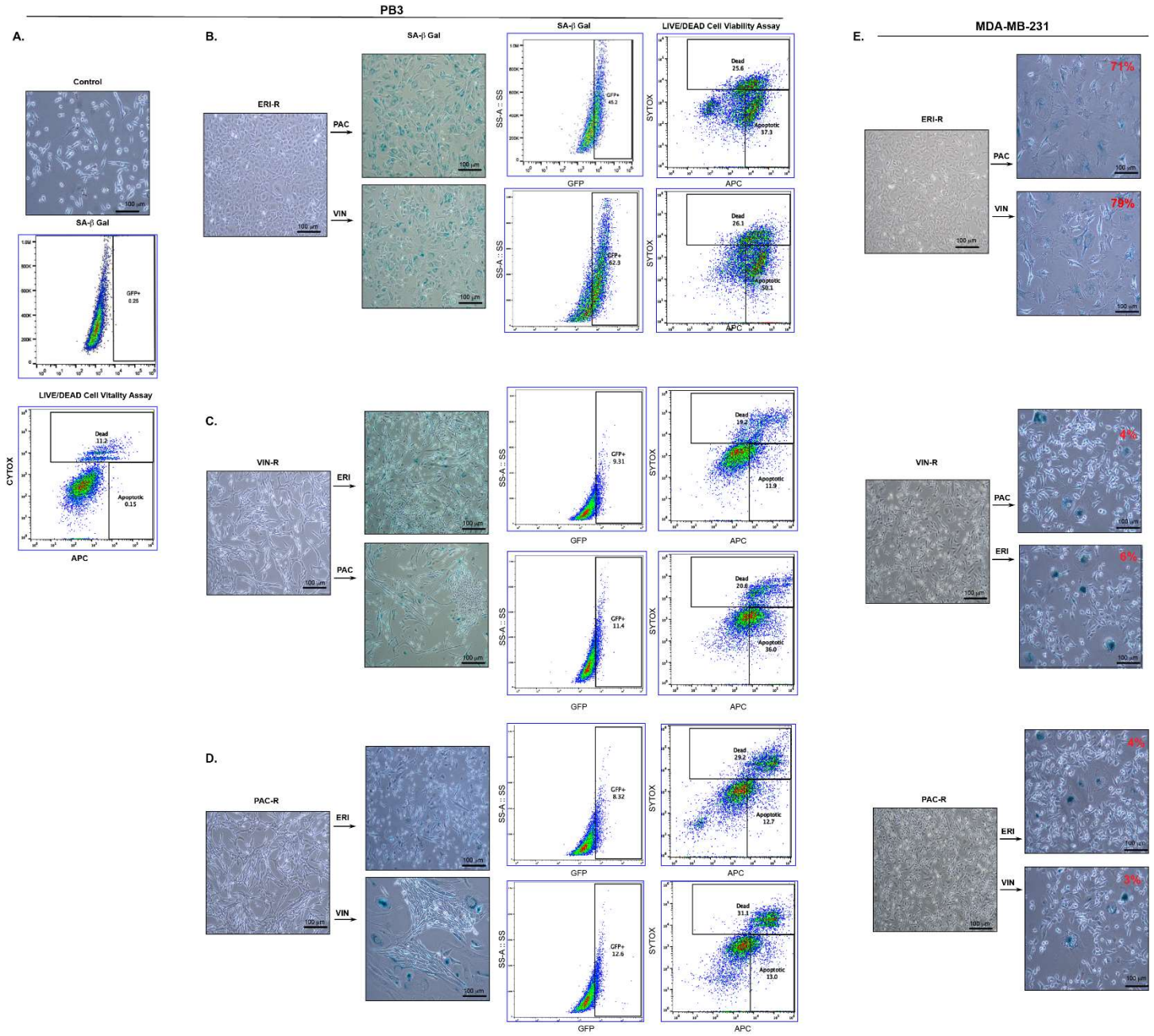

Supplementary Figure S5: Primary eribulin treatment sensitizes TNBC cells to other chemotherapeutics. (A) PB3 cells were analyzed using senescence-associated beta-galactosidase assay (top flow cytometry panel) and SYTOX for live/dead/apoptotic cells (lower flow cytometry panel). **(B-D)** $PB3^{ERI\text{-}R}$ cells were treated +/- paclitaxel or vinorelbine. $PB3^{PAC\text{-}R}$ cells were treated +/- eribulin or vinorelbine. $PB3^{VIN\text{-}R}$ cells were treated +/- paclitaxel or eribulin. After 48 h, cells were analyzed as in (A). **(E)** Senescence-associated beta-galactosidase assay was used to analyze MDA-MB-$231^{ERI\text{-}R}$, MDA-MB-$231^{PAC\text{-}R}$, and MDA-MB-$231^{VIN\text{-}R}$ cells as in (A). Related to Figure 6.

A.

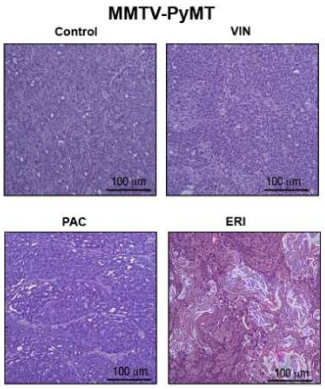

B.

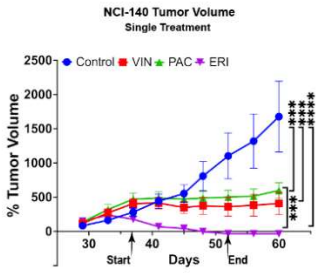

C.

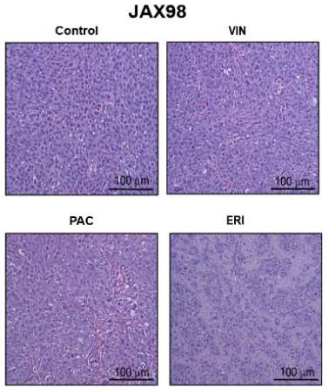

D.

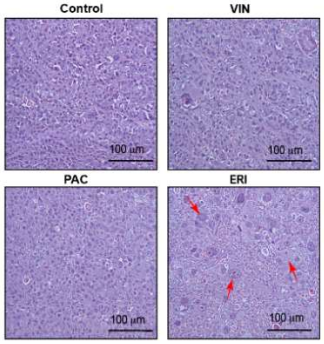

E.

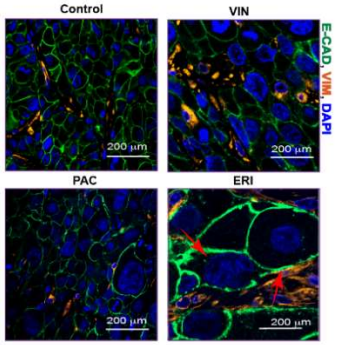

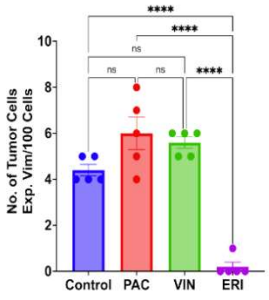

F.

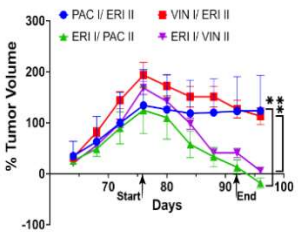

G.

NCI-140 Metastasis				
Group	Lung	Liver	Ovary	lymph node
Control	1/5	0/5	5/5	1/5
E1P2	0/5	0/5	0/5	0/5
E1V2	0/5	0/5	0/5	0/5
P1E2	0/5	0/5	1/5	0/5
V1E2	0/5	0/5	1/5	0/5

H.

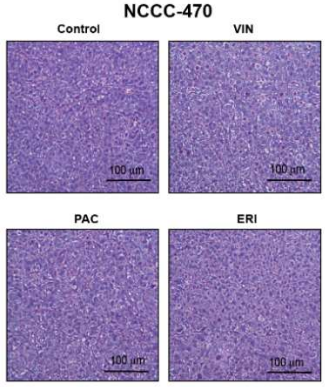

I.

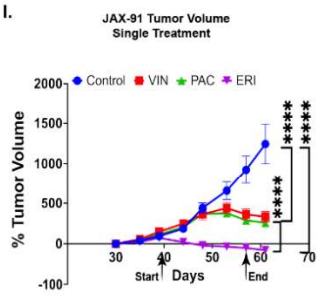

J.

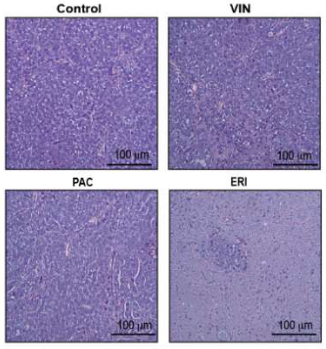

K.

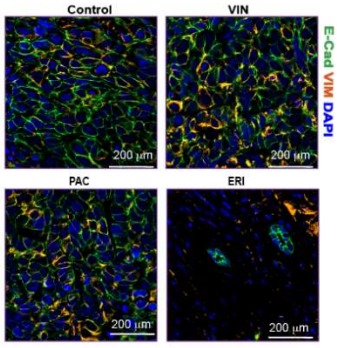

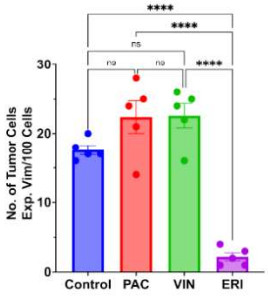

L.

JAX-91				
Group	Lung	Liver	Ovary	lymph node
Control	0/0	3/5	4/5	4/5
E1P2	0/0	0/0	1/5	2/5
E1V2	0/0	0/0	0/0	1/5
P1E2	0/0	0/0	4/5	4/5
V1E2	0/0	0/0	2/5	2/5

M.

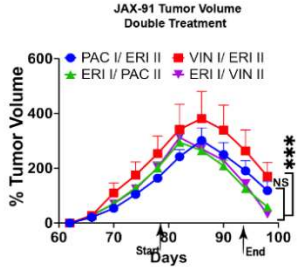

Supplementary Figure S6: MET induction is accompanied by robust tumor regression and reduced metastatic burden. (A) H&E histology of representative MMTV-PyMT tumors harvested after 2 wk of treatment followed by a 1-wk drug holiday. **(B)** Mice bearing orthotopic NCI-140^{naïve} tumors were treated with single agents as indicated. Tumor volumes are shown as mean of 10 tumors +/- SD. **(C)** H&E histology of JAX-98^{naïve} tumors harvested from mice treated as a (A). **(D)** H&E histology of NCI-140^{naïve} tumors harvested from mice treated as a (A). **(E)** NCI-140^{naïve} tumors harvested from mice treated as in (A) were used for immunofluorescence for E-cadherin (green) and vimentin (red). **(F)** Mice bearing bilaterally-implanted orthotopic NCI-140^{naïve} tumors were treated with paclitaxel, eribulin, or vinorelbine for 2 wk followed by a 1-week holiday. One tumor was surgically resected, and mice were maintained until the remaining tumor resumed growth. Mice were then treated with a different drug as indicated. Tumor volumes were analyzed as in (B) and are shown as mean of 5 tumors +/- SD. **(G)** In mice with NCI-140^{naïve} xenografts treated as in (F), after the secondary drug treatment the remaining tumor was surgically resected. Mice were then maintained for 3 months before organs were harvested for evaluation of metastasis. Distribution patterns of metastasis are noted. **(H)** H&E histology of NCCC-470^{NAC} tumors harvested from mice treated as a (A). **(I)** Mice bearing orthotopic JAX-91^{NAC} tumors were treated with single agents as indicated and analyzed as in (B). **(J)** H&E histology of JAX-91^{NAC} tumors harvested from mice as in (C). **(K)** JAX-91^{NAC} tumors harvested from mice treated as in (A) were used for immunofluorescence as in (E). **(L-M)** Mice bearing bilaterally-implanted JAX-91^{NAC} tumors were treated and analyzed as in (F/G). Panel (M) shows tumor volumes as mean of 5 +/- SD. *$p<0.05$, **$p<0.001$, ***$p<0.0005$, ****$p<0.0001$ by Tukey-adjusted pairwise comparison. Related to Figure 7.

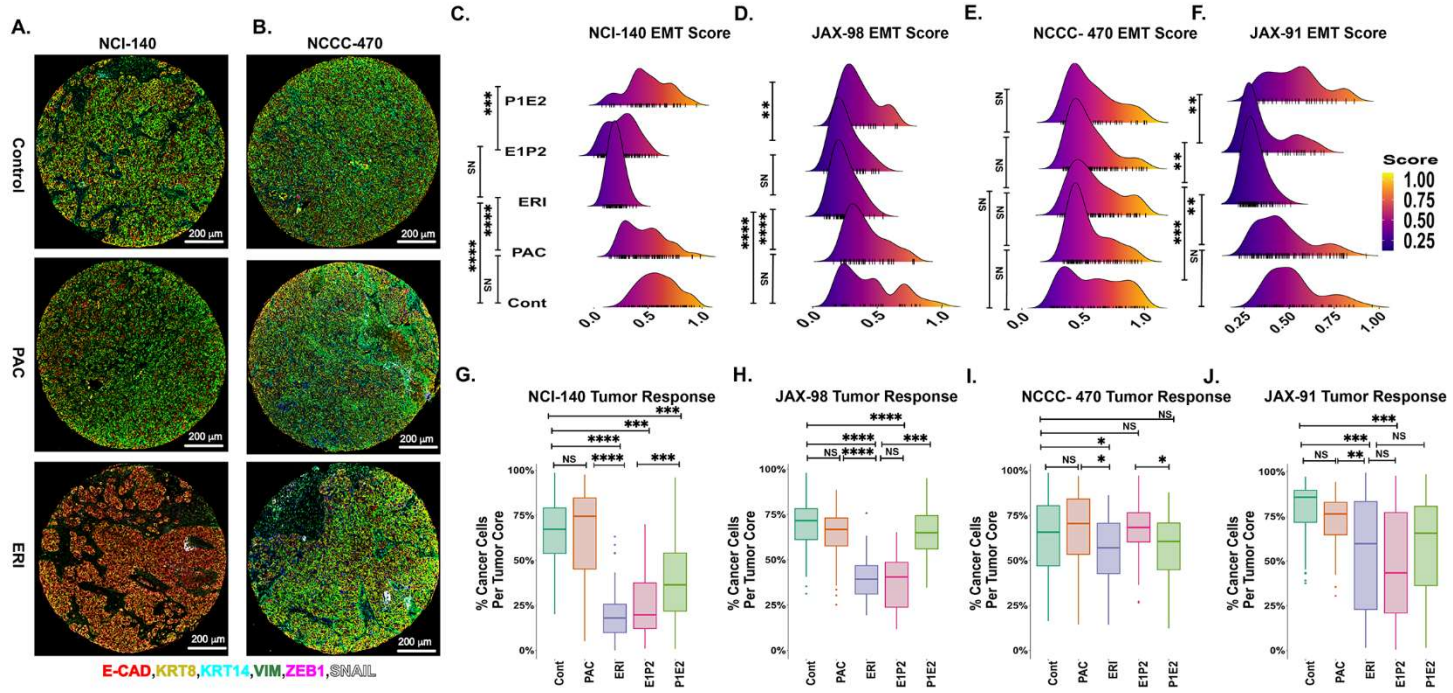

Supplementary Figure S7: Eribulin reverses EMT in PDX tumors. (A/B) Representative images of multiplexed immunostaining of EMT markers in PDX tumors from mice treated as indicated. (C-F) EMT scores were generated using images as in (A/B) from 5 tumors per group and ≥100 microscopic fields/tumor. Each histogram reflects scores from ≥500 fields. (G-J) inForm image analysis was used to quantify proportions of cancer and stromal cells within tumor sections processed as above. *p<0.05, *p<0.001, ***p<0.0005, ****p<0.0001 by Tukey-adjusted pairwise comparison.